Available online at www.sciencedirect.com
SCIENCE DIRECT
Journal of Magnetic Resonance 179 (2006) 299–307
JMR Journal of Magnetic Resonance
www.elsevier.com/locate/jmr

Communication

Insight into the CSA tensors of nucleobase carbons in RNA polynucleotides from solution measurements of residual CSA: Towards new long-range orientational constraints

Alexandar L. Hansen, Hashim M. Al-Hashimi *

Department of Chemistry and Biophysics Research Division, The University of Michigan, Ann Arbor, MI 48109, USA

Received 9 November 2005; revised 30 December 2005
Available online 23 January 2006

Abstract

Using residual chemical shift anisotropies (RCSAs) measured in a weakly aligned stem–loop RNA, we examined the carbon chemical shift anisotropy (CSA) tensors of nucleobase adenine C2, pyrimidine C5 and C6, and purine C8. The differences between the measured RCSAs and the values back-calculated using three nucleobase carbon CSA sets [D. Stueber, D.M. Grant, 13C and (15)N chemical shift tensors in adenosine, guanosine dihydrate, 2′-deoxythymidine, and cytidine, J. Am. Chem. Soc. 124 (2002) 10539–10551; D. Sitkoff, D.A. Case, Theories of chemical shift anisotropies in proteins and nucleic acids, Prog. NMR Spectrosc. 32 (1998) 165–190; R. Fiala, J. Czernek, V. Sklenar, Transverse relaxation optimized triple-resonance NMR experiments for nucleic acids, J. Biomol. NMR 16 (2000) 291–302] reported previously for mononucleotides (1.4 Hz) is significantly smaller than the predicted RCSA range (−10–10 Hz) but remains larger than the RCSA measurement uncertainty (0.8 Hz). Fitting of the traceless principal CSA values to the measured RCSAs using a grid search procedure yields a cytosine C5 CSA magnitude ($CSA_a = (3/2 \cdot (\delta_{11}^2 + \delta_{22}^2 + \delta_{33}^2))^{1/2} = 173 \pm 21$ ppm), which is significantly higher than the reported mononucleotide values (131–138 ppm) and a guanine C8 CSA_a (148 ± 13 ppm) that is in very good agreement with the mononucleotide value reported by solid-state NMR [134 ppm, D. Stueber, D.M. Grant, 13C and (15)N chemical shift tensors in adenosine, guanosine dihydrate, 2′-deoxythymidine, and cytidine, J. Am. Chem. Soc. 124 (2002) 10539–10551]. Owing to a unique sensitivity to directions normal to the base plane, the RCSAs can be translated into useful long-range orientational constraints for RNA structure determination even after allowing for substantial uncertainty in the nucleobase carbon CSA tensors.

Keywords: Chemical shielding tensor; Nucleic acids; ^{13}C spin relaxation; RCSA; Residual dipolar couplings

1. Introduction

Circulation of current within electronic clouds of molecules gives rise to a local magnetic field at nuclei of interest that fluctuates as molecules tumble relative to the applied magnetic field. The orientational dependence of this local field can be mathematically described by five elements of a 2nd rank chemical shift anisotropy (CSA) tensor. Knowledge of CSA tensors is required to account for CSA relaxation mechanisms. This proves to be important for a range of biomolecular NMR applications including the interpretation of spin relaxation data in terms of angular constraints [1–4] and dynamical parameters [5,6] and in analyzing TROSY effects [7]. Knowledge of CSA tensors is also necessary for structure determination by solid-state NMR [8–10] and for interpreting spectra of partially oriented samples in which anisotropic chemical shift interactions no longer average to zero [11–15].

Of particular interest in nucleic acids are the CSAs of the nucleobase carbons adenine C2, pyrimidine C5 and C6, and purine C8 (Fig. 1A). These C–H carbons are essential spins for probing the fast dynamics of nucleic acids by spin relaxation measurements [16–21]. Unlike amide nitrogens in proteins, imino ^{15}N relaxation data is only available

* Corresponding author. Fax: +1 734 647 4865.
E-mail address: hashimi@umich.edu (H.M. Al-Hashimi).

1090-7807/$ - see front matter © 2006 Elsevier Inc. All rights reserved.
doi:10.1016/j.jmr.2005.12.012

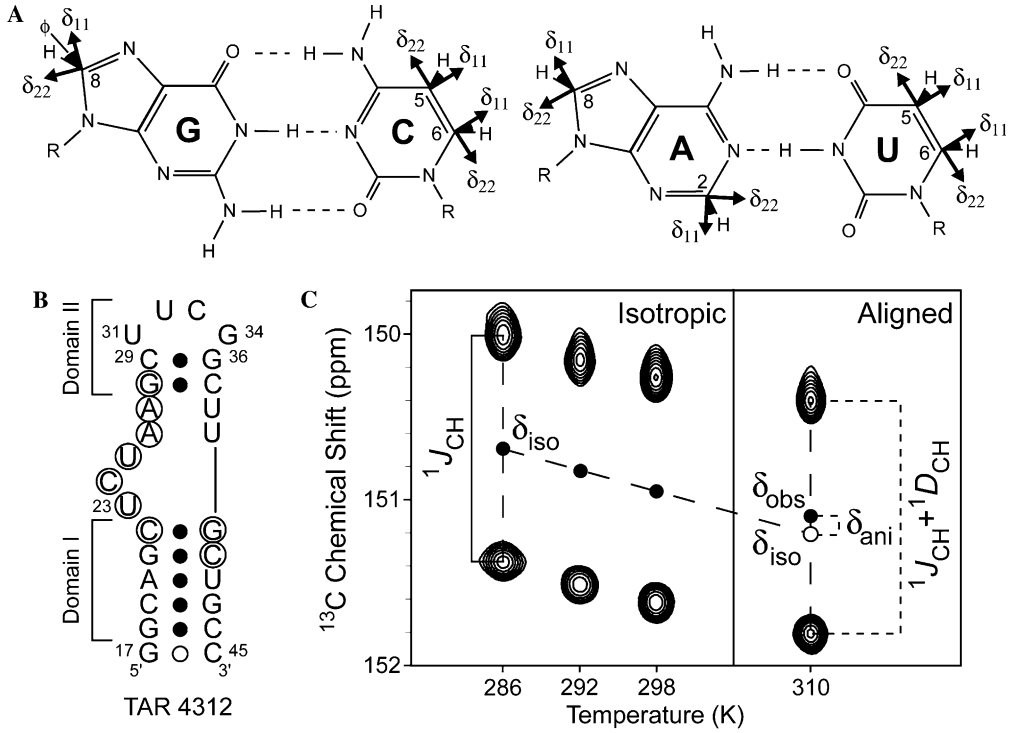

Fig. 1. Simultaneous measurements of nucleobase RDCs and RCSAs in TAR4312 RNA. (A) Watson–Crick base-pairs showing the nucleobase carbons targeted for RCSA measurements along with the definition of the angle Φ (shown as positive values) used in Table 1 to define the orientation of the δ_{11}/δ_{22} CSA principal axes. (B) Secondary structure of TAR4312 in which A22-U40, G26-C39 and the CUGGGA hairpin loop in wt-TAR are replaced with C22-G40, A26-U39, and a UUCG loop, respectively. Filled circles denote Watson–Crick hydrogen bonding as inferred from a J_{NN}-COSY experiment [39]. Residues that experience the largest bicelle-induced perturbations in isotropic ^{13}C chemical shifts are circled. (C) Measurements of base RDCs ($^1D_{CH}$) and RCSAs (δ_{ani}) using C2 in A26 as an example. Uniformly ^{15}N/^{13}C-labeled TAR4312 was prepared by in vitro transcription. NMR samples contained ~0.5 mM RNA, 15 mM sodium phosphate, pH 6.4, 0.1 mM EDTA, and 25 mM NaCl in D_2O. NMR experiments were carried out on a Bruker AMX 600 MHz spectrometer equipped with a cryogenic probe.

for half the residues in nucleic acids (guanine and uridine/thymine) and seldom for flexible sites of interest due to rapid exchange of imino protons with solvent [22]. The large CSA of these aromatic carbons together with the often highly anisotropic tumbling of nucleic acids makes knowledge of all five CSA tensor elements crucial for these studies especially when working at higher magnetic fields.

To date, only one solid-state NMR study of RNA mononucleotide powders has reported experimental values for the principal components of the nucleobase carbon CSAs (Table 1, SS) [23]. However, the CSA orientations were obtained using density functional theory (DFT) calculations on simplified mononucleotides. To our knowledge, no experimental data has been obtained so far that reports on the orientation of the carbon nucleobase CSAs. Two other nucleobase carbon CSA sets derived by DFT calculations on simplified mononucleotides and which include both principal values and orientations have also been reported in the literature (Table 1, DFT1 [24] and DFT2 [25]). Though widely used in the analysis of ^{13}C relaxation data, the validity of these mononucleotide CSAs in the context of RNA polynucleotides under solution conditions remains to be established. This is important given the well-known dependence of CSAs on intermolecular interactions [23,24,26,27] and involvement of nucleobases in hydrogen-bonding and stacking interactions. Indeed, a recent ^{13}C relaxation study of RNA dynamics alludes to potential deviations from the mononucleotide CSAs. In particular, difficulties were encountered when using the SS CSAs in analyzing ^{13}C relaxation data measured at high (17.6 T) but not low (11.7 T) magnetic fields [21]. Furthermore, the discrepancies in the reported CSA magnitudes ($CSA_a = (3/2 \cdot (\delta_{11}^2 + \delta_{22}^2 + \delta_{33}^2))^{1/2}$, where δ_{ii} are the principal values of the traceless CSA tensor) for purine C8 and pyrimidine C6 are sufficiently large to impart undesirable uncertainty in the dynamical interpretation of relaxation data (Table 1).

Here, we have measured the manifestation of nucleobase carbon CSAs as residual perturbations in chemical shifts that can be observed when a weak degree of RNA alignment is imposed [13–15,28–30]. Such residual chemical shift anisotropies (RCSAs) have previously been used to determine CSA tensors for carbonyl carbons, amide nitrogens, and amide protons in proteins [13,28] and more recently for sugar carbons in A-form RNA helices [15]. Since RCSAs depend on the orientation of CSA tensors relative to the order tensor governing alignment, they also provide long-range orientational constraints [14,31] for structure determination, much like residual dipolar couplings (RDCs) [32,33]. Having an abundance of such long-range

Table 1
Analysis of nucleobase carbon CSAs using RCSAs measured in TAR4312

Atom (#)	Source	δ_{11} (ppm)	δ_{22} (ppm)	δ_{33} (ppm)	ϕ (deg)	CSA$_a$ (ppm)	rmsd (Hz)	Q (%)
A C2 (1)	SS	84.7	3.6	−88.3	−3.0	149.9	1.8 (1.4)	44 (36)
	DFT1	84.0	1.0	−85.0	−3.8	146.4	1.6 (1.2)	40 (31)
	DFT2	82.1	1.8	−83.9	−3.6	143.8	1.6 (1.2)	41 (32)
C C5 (4)	SS	80.1	−1.2	−78.9	−11.0	137.7	1.6 (1.4)	43 (38)
	DFT1	82.0	−11.0	−71.0	−9.6	133.5	1.9 (1.7)	55 (49)
	DFT2	80.6	−11.2	−69.4	−8.9	131.0	1.9 (1.8)	56 (53)
	RCSA	107.4 ± 21.4	−18.0 ± 24.2	−89.4 ± 7.5	38.2 ± 13.3	172.6 ± 21.2	0.6	14
	Calc-4	± 20.3	± 19.0	± 7.4	(−90 to 90)	± 17.7	—	—
U C5 (2)	DFT1	80.3	−7.6	−72.7	10.7	133.0	1.7 (1.6)	51 (48)
	DFT2	76.5	−7.0	−69.5	10.6	126.9	2.0 (1.9)	63 (60)
C C6 (2)	SS	98.4	9.1	−107.5	31.0	178.8	0.9 (1.0)	19 (22)
	DFT1	94.0	−7.0	−87.0	19.8	157.1	1.4 (0.9)	34 (22)
	DFT2	98.3	14.2	−112.5	26.9	183.9	1.4 (1.4)	30 (30)
U C6 (2)	DFT1	102.7	−14.4	−88.3	19.3	166.8	0.6 (0.2)	14 (5)
	DFT2	105.4	1.8	−107.2	28.3	184.1	1.3 (1.3)	30 (30)
A C8 (1)	SS	78.3	−1.6	−76.7	−27.0	134.3	0.5 (0.2)	14 (6)
	DFT1	71.3	−13.6	−57.7	−21.2	113.6	0.1 (0.1)	3 (3)
	DFT2	72.5	−3.5	−69.0	−29.4	122.8	0.1 (0.2)	3 (6)
G C8 (5)	SS	76.0	3.0	−79.0	−28.0	134.3	1.7 (1.4)	48 (40)
	DFT1	71.7	−15.4	−56.3	−21.6	113.2	1.4 (1.2)	49 (42)
	DFT2	73.1	−9.8	−63.3	−30.4	119.0	1.5 (1.2)	49 (39)
	RCSA	97.8 ± 11.8	−37.1 ± 12.2	−60.7 ± 4.0	−1.8 ± 6.9	148.1 ± 12.8	0.6	16
	Calc-5	± 16.9	± 19.3	± 6.9	(−90 to 90)	± 14.7	—	—

The number of RCSAs measured is shown in parentheses next to the residue/carbon type. Shown are the principal values (δ_{11}, δ_{22}, δ_{33}), orientation (ϕ, see also Fig. 1A), and magnitude ($\mathrm{CSA}_a = (3/2 \cdot (\delta_{11}^2 + \delta_{22}^2 + \delta_{33}^2))^{1/2}$) of the traceless CSA tensor reported by solid state NMR (SS) [23] and DFT calculations from Sitkoff et al. (DFT1) [24] and Fiala et al. (DFT2) [25]). In all cases, δ_{33} is oriented normal to the base plane. The mean and standard deviation in CSA parameters derived from a grid-search employing the measured RCSAs ("RCSA") is shown. The standard deviations reflect uncertainty in the RCSA measurements (0.8 Hz), base orientations (±6°), and the domain specific order tensors (±5% and ±0.1 in GDO and η, respectively). The corresponding standard deviations obtained when using synthetic RCSAs is also shown ("Calc") and was used to gauge how well the RCSAs can intrinsically define the CSA parameters given the latter uncertainties. The entire range of accepted ϕ angles are shown for "Calc." The root-mean-square-deviation (rmsd) and quality factor (Q) [15,48] for a given carbon type is shown when comparing the measured RCSAs with values back-calculated using an order tensor derived using RDCs and the RDC-validated domain structures. The best-fit results (rmsd and Q-factor) following ±5%, ±0.1, and ca. 6° variations in the order tensor GDO [49], order tensor asymmetry η, and orientation of individual bases are shown in parenthesis. For the single adenine C2 and C8 RCSA, only the difference between the measured and predicted values was used to compute rmsd and Q.

constraints is particularly important for structure determination of extended and proton deficient nucleic acids.

2. Results and discussion

Our study was carried out on a uniformly $^{13}C/^{15}N$ labeled mutant of the transactivation response element (TAR4312) RNA (Fig. 1B) which was partially aligned using a 5% (w/v) DHPC:DMPC (3:1) bicelle medium [32,34] that forms an aligned liquid crystalline phase at temperatures above 298 K [35]. At or below room temperature the bicelles form an isotropic phase, allowing the measurement of the isotropic chemical shifts, their temperature dependences, and scalar couplings. One bond C–H splittings and ^{13}C chemical shifts were measured simultaneously from the difference and average frequency respectively of the upfield and down field components of the $\{^{13}C\}$–H doublet (Fig. 1C). These components were measured in separate sub-spectra using 2D ^{13}C–^{1}H S^3E HSQC experiments [36,37]. The RDCs were computed from the difference in C–H splittings measured in aligned (T = 310 K) and isotropic ($T = 292$ K) phases (Fig. 1C). Due to the temperature dependence of isotropic chemical shifts (δ_{iso}), the RCSAs could not simply be computed from the difference in chemical shifts measured at 298 and 310 K. Rather, the value of δ_{iso} at 310 K ($\delta^{310K}_{iso,bicelle}$) was determined by linearly extrapolating δ_{iso} measured in the isotropic phase (286, 292, and 298 K) to 310 K (Figs. 1C and 2A). This approach was previously used to measure RCSAs in the protein ubiquitin [13]. The chemical shifts measured in the aligned phase ($\delta^{310K}_{obs,bicelles} = \delta^{310K}_{iso,bicelle} + \delta^{310K}_{ani}$) were also corrected to account for changes in the lock frequency due to quadrupolar ^2H splittings (7.6 Hz). The RCSAs were then computed by subtracting $\delta^{310K}_{iso,bicelle}$ from $\delta^{310K}_{obs,bicelles}$. The RDCs and RCSAs measured in TAR4312 are listed in Table 2.

Besides assuming a linear temperature dependence for δ_{iso} over 286–310 K, which was observed for all carbons examined (e.g., Fig. 2A), the latter approach for measuring RCSAs assumes no TAR4312 alignment at $T \leqslant 298$ K.

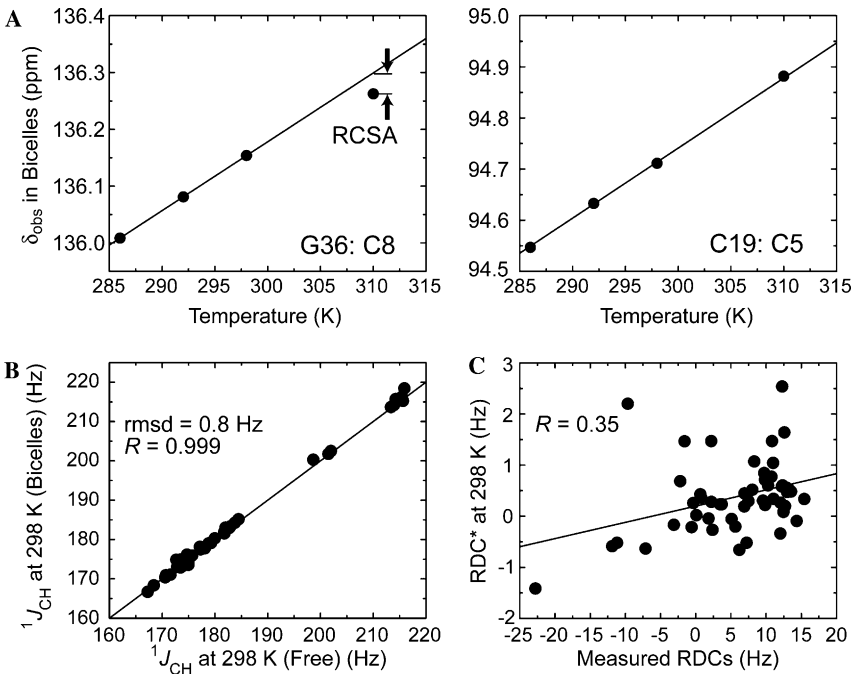

Fig. 2. Measurement of nucleobase RCSAs in TAR4312 weakly aligned in a bicelle medium. (A) Measurement of RCSAs in bicelles using a linear extrapolation of the temperature dependence of isotropic ^{13}C chemical shifts. Shown are two examples from domains I and II. (B and C) Lack of TAR4312 alignment in bicelles at $\leqslant$310 K. (B) Correlation plot between one bond C–H splittings measured at 298 K in the presence and absence of bicelles. (C) Correlation plot between measured RDCs (RDC = 310–298 K) and "would be RDCs" (RDC* = 298 K in bicelles − 298 K without bicelles).

Any unaccounted for residual TAR4312 alignment would lead to underestimation of the RCSAs and ultimately their associated CSAs. Negligible TAR4312 alignment at $\leqslant$298 K was confirmed based on a number of observations. First, no quadrupolar ^{2}H splittings were observed at $\leqslant$298 K. Second, the differences between C–H splittings measured in the presence and absence of bicelles at 298 K (root-mean-square-deviation, rmsd = 0.8 Hz, Fig. 2B) are within the estimated measurement uncertainty (0.9 Hz, see legend of Table 2). Finally, a poor correlation ($R = 0.35$) is observed between the measured RDCs and "would be RDCs" at 298 K (Fig. 2C).

As shown in Fig. 3, we observed significant bicelle-induced perturbations in δ_{iso} (rmsd = 8.4/7.2/5.5 Hz at 292, 298, 310 K) which precluded measurements of RCSAs as the difference between chemical shifts observed in the presence and absence of bicelles. The latter approach was previously used to measure ^{31}P RCSAs in DNA [14] and ^{13}C RCSAs in RNA [15] but using the Pf1-phage ordering medium [38,39]. The bicelle-induced perturbations in TAR4312 are particularly pronounced for structurally unstable regions (Fig. 1B, circled residues) including the bulge (U23, C24, and U25) and two neighboring adenines in domain II (A26 and A27) that based on J_{NN}-COSY experiments [40] are not involved in A-U Watson–Crick hydrogen bonding (data not shown). Interestingly, these residues also have carbon chemical shifts that have markedly different temperature dependencies in the presence and absence of bicelles (Fig. 3, inset). These perturbations likely arise from changes in the structural dynamics of TAR4312 due to transient contacts with the bicelles. Similar perturbations have been reported for fraying terminal residues in a duplex RNA in Pf1-phage [15]. These results underscore the importance of accommodating ordering media induced changes in δ_{iso} when measuring RCSAs and suggest that the bicelle medium can affect the conformational dynamics of flexible RNAs.

The RCSA (δ_{ani}) measured for a carbon nucleus k depends on the magnitude and orientation of the kth CSA tensor (δ_{ij}^{k}) relative to the order tensor (S_{ij}) governing alignment [41]

$$\delta_{ani}(k) = (\delta_{obs} - \delta_{iso}) = \frac{2}{3}\sum_{ij=\{x,y,z\}} S_{ij}\delta_{ij}^{k}. \quad (1)$$

To interpret RCSAs using Eq. (1), we first used RDCs to validate domain structures for TAR4312 and determine their order tensors. The domain structures comprised idealized A-form helices and a previous X-ray structure [42] of the U31U32C33G34 tetraloop (Fig. 1B). The local structure of these domains has previously been validated using RDCs measured in free TAR [43] and for TAR bound to four distinct ligands that target the bulge and neighboring residues without affecting the remaining local helical structure [44–46]. The 108 RDCs belonging to TAR residues that coincide with those of TAR4312 fit (using SVD [41]) the above domain structures with an overall rmsd (normalized to reflect the TAR4312 degree of order) of 1.5 Hz (Fig. 4A). As shown in Fig. 4B, the agreement between the RDCs measured in TAR4312 and these model structures is equally good with the overall rmsd in the SVD fit

Table 2
RDCs and RCSAs in TAR4312 measured at a ^{1}H spectrometer frequency of 600 MHz

Residue	Atom/vector	RCSA (Hz)	RDC (Hz)
G18	C8/C8-H8	4.1 ± 0.8	−1.4 ± 1.4
C19	C5/C5-H5	0.8 ± 0.8	−9.2 ± 1.4
A20	C2/C2-H2	−2.5 ± 0.8	13.6 ± 1.4
A20	C8/C8-H8	−3.6 ± 0.8	13.5 ± 1.4
G21	C8/C8-H8	−3.5 ± 0.8	11.6 ± 1.4
C22	C5/C5-H5	−4.9 ± 0.8	12.7 ± 1.4
C22	C6/C6-H6	−5.1 ± 0.8	2.3 ± 1.4
G28	—/C1′-H1′	—	−14.9 ± 1.4
G28	C8/C8-H8	−3.2 ± 0.8	13.5 ± 1.4
C29	C5/C5-H5	−6.4 ± 0.8	12.8 ± 1.4
C29	C6/C6-H6	−7.4 ± 0.8	11.7 ± 1.4
U31	—/C1′-H1′	—	−0.2 ± 1.4
U31	C5/C5-H5	−7.6 ± 0.8	13.7 ± 1.4
U31	C6/C6-H6	−7.4 ± 0.8	11.9 ± 1.4
U32	—/C1′-H1′	—	4.6 ± 1.4
C33	—/C1′-H1′	—	−0.4 ± 1.4
G34	—/C1′-H1′	—	7.5 ± 1.4
G34	C8/C8-H8	−6.9 ± 0.8	9.0 ± 1.4
G36	C8/C8-H8	−5.5 ± 0.8	13.2 ± 1.4
C37	—/C1′-H1′	—	3.2 ± 1.4
G40	C8/C8-H8	−2.1 ± 0.8	3.6 ± 1.4
C41	C5/C5-H5	−5.9 ± 0.8	7.5 ± 1.4
U42	C5/C5-H5	−3.1 ± 0.8	1.2 ± 1.4
U42	C6/C6-H6	−4.7 ± 0.8	13.5 ± 1.4
G43	C8/C8-H8	−5.6 ± 0.8	16.7 ± 1.4
C44	—/C1′-H1′	—	14.5 ± 1.4

The RDC measurement uncertainty was obtained by multiplying the observed rmsd between splittings measured at 292 and 298 K (0.9 Hz) by $2^{1/2}$. The RCSA measurement uncertainty was obtained by propagating the errors in $\delta^{310K}_{obs,bicelle}$ and $\delta^{310K}_{iso,bicelle}$. The $\delta^{310K}_{obs,bicelle}$ uncertainty (0.3 Hz) was obtained from the rms of residuals in the three point linear-fit of δ_{iso} vs. temperature (Fig. 2A). The $\delta^{310K}_{iso,bicelle}$ uncertainty was obtained using the following procedure. Perfect synthetic data corresponding to δ_{iso} at 286, 292, and 298 K was generated. Each data point was then perturbed by an amount chosen randomly from a Gaussian distribution centered at zero with the standard deviation set to the rms in the three-point residuals. Linear extrapolation of the resulting data set to 310 K was then used to compute an error in $\delta^{310K}_{iso,bicelle}$. The error was obtained from the standard deviation in $\delta^{310K}_{iso,bicelle}$ following thousands of such runs (0.7 Hz).

[41] (1.5 Hz) being approximately equal to the estimated RDC measurement uncertainty (1.4 Hz, see legend of Table 2).

Next, we examined the agreement between the measured RCSAs and values back-calculated using Eq. (1), the RDC-validated domain structures, RDC-derived domain-specific order tensors and each of the DFT1, DFT2, and SS nucleobase carbon CSAs. The analysis that follows assumed uniform CSAs from site to site and that internal motions uniformly scale all of the measured RDCs (and derived order tensors) and RCSAs by a similar amount. Furthermore, the bond lengths reported by Cornell et al. [47] ($r_{CH(base)} = 1.08$ Å and $r_{C1'H1'} = 1.09$ Å) were assumed in the RDC-determination of the order tensors. Any systematic under-/over-estimation of these bond lengths will lead to under-/over-estimation of the degree of order and hence predicted RCSAs. It should be noted at the outset that most of the DFT1, DFT2, and SS CSA tensor elements are in very good agreement with one another especially the orientations (Table 1). In all cases, the most shielded component (δ_{33}) is oriented perfectly along the base normal and the least shielded component (δ_{11}) close to coincident ($\phi < 30°$) with the corresponding C–H bond (Table 1). However, for a subset of carbons, particularly pyrimidine C6 and purine C8, large differences in the principal values are observed leading to differences in CSA_a as large as 27 ppm.

Shown in Fig. 4C are correlation plots showing the RCSAs measured in Watson–Crick base-pairs and values back-calculated using the mononucleotide CSAs. Similar overall agreement is observed for the three CSA sets with the best agreement observed for DFT1 and SS followed by DFT2. Similar agreement was observed when combining the RDCs and RCSAs in the SVD fit ($rmsd_{RDC}$ (Hz)/$rmsd_{RCSA}$ (Hz) = 1.5/1.3, 1.5/1.2, and 1.4/1.4 for SS, DFT1 and DFT2, data not shown). Although the observed agreement (rmsd = 1.3–1.4 Hz) is favorable considering that the differences between measured and predicted RCSAs are almost an order of magnitude smaller than the predicted RCSA range (ca. −10–10 Hz), the differences remain higher than the estimated RCSA measurement uncertainty (0.8 Hz, see legend of Table 2).

Shown in Table 1 is the rmsd and quality factor (Q) [15,48] describing the level of agreement between the measured and predicted RCSAs for individual carbon types.

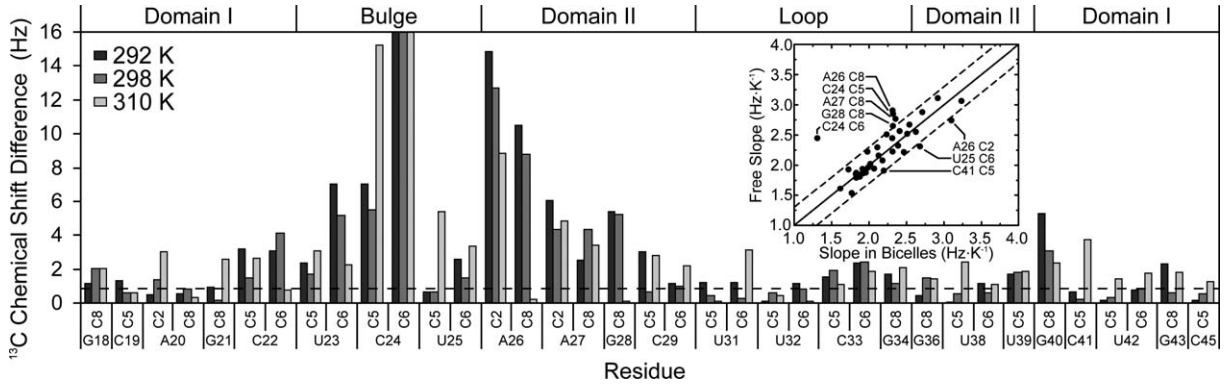

Fig. 3. Residue specific bicelle-induced perturbations in isotropic ^{13}C chemical shifts in TAR4312. Shown are the differences between C2 (adenine), C5 (pyrimidine), C6 (pyrimidine), and C8 (purine) chemical shifts measured in the presence and absence of bicelles at $T = 292$, 298, and 310 K. (Inset) Corresponding slopes of the ^{13}C chemical shift vs. temperature.

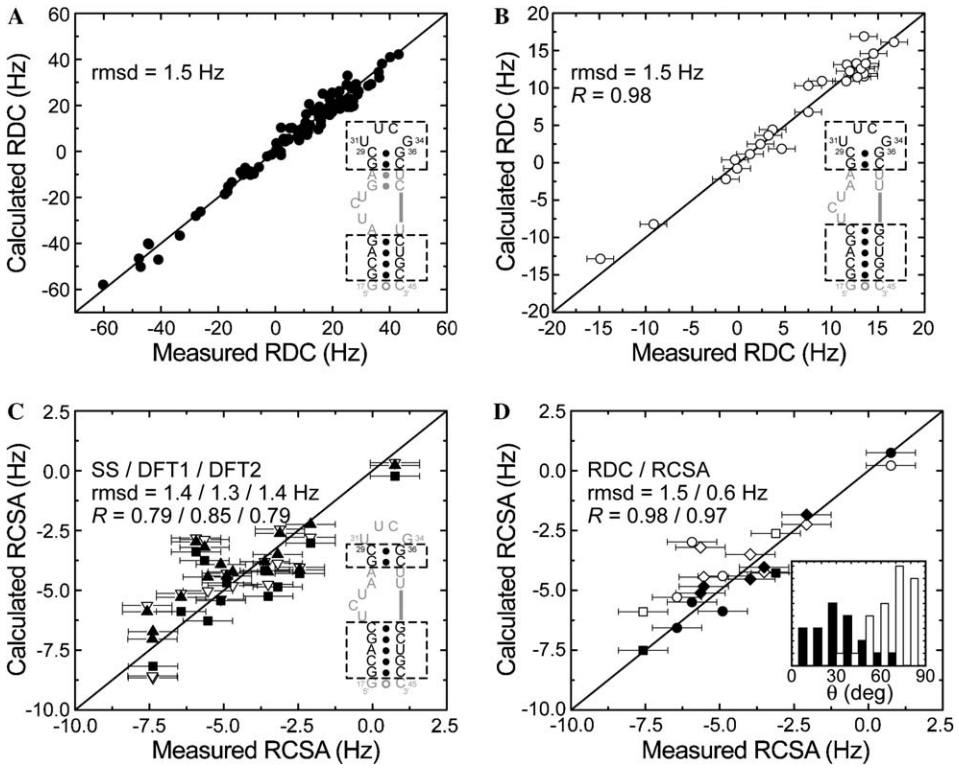

Fig. 4. Evaluating nucleobase CSA tensors using RCSAs. (A and B) RDC-based validation of model structures for the two TAR4312 domains comprising idealized A-form helices for hydrogen bonded Watson–Crick residues and an X-ray structure [42] for the UUCG tetraloop. (A) Correlation plot between 108 RDCs previously measured for TAR in the free state [43] and when bound to four distinct ligands [44–46] and values back-calculated using best-fit order tensors determined independently for each domain using the assumed model domain structures and a modified version of ORDERTEN_SVD [41]. Only RDCs belonging to TAR residues that coincide with those of TAR4312 were included in the fit. (B) Corresponding correlation plot between measured and back-calculated RDCs in TAR4312. A total 13/13 RDCs in domains I/II with condition numbers of 3.7/2.6 were used in the latter SVD fit. The idealized A-form helices were generated using Insight II (molecular simulations) with propeller twist angles set to $-15°$ [54]. (C) Correlation plot between measured RCSAs and values back-calculated using the RDC-derived order tensor, and SS (filled squares), DFT1 (filled triangles), and DFT2 (open triangles) CSAs. (D) Same as in (B) for cytosine C5 (filled circles) and guanine C8 (filled diamonds) when using the RCSA-fitted CSAs. Also shown is the fit between measured uridine C5 RCSAs and values back-calculated when assuming the RCSA-derived cytosine C5 CSA (filled squares). For comparison, the corresponding agreement with DFT1 is shown using open symbols. (Inset) The angle (θ) between the principal axis of the order tensor (S_{zz}) and C–H RDC vectors (in white) and δ_{33} CSA axis (in black) in TAR4312. In all cases, RDCs and RCSAs from flexible residues (domain I G17-C45, domain II A26-U39 and A27-U38, loop U32 and C33 [20,55]) were excluded from above analysis. The error bars denote the estimated uncertainty in RDCs (1.4 Hz) and RCSAs (0.8 Hz).

We focus on cytosine C5 and guanine C8 for which more than two RCSA measurements were available (Table 1). Poor agreement is observed for these carbons with all three mononucleotide CSAs ($Q > 40\%$). This is the case even after allowing the input order tensor parameters to vary within their experimental uncertainty ($\pm 5\%$ and ± 0.1 variations in the generalized degree of order, GDO [49], and asymmetry η, respectively) and allowing the orientation of individual nucleobases to vary randomly by ca. 6° (Table 1, shown in parentheses). The latter was used to account for structural noise and was accomplished by applying random Euler rotations independently to each base. This suggests that some of the scatter in Fig. 4C is due to deviations from the assumed mononucleotide guanine C8 and cytosine C5 CSAs. Indeed, better agreement is observed when excluding the latter RCSAs from the fit of Fig. 4C (rmsd (Hz)/$R = 1.2/0.95$; 1.1/0.88; and 1.2/0.96 for SS, DFT1, and DFT2, respectively).

To this end, we carried out an exhaustive three-parameter (δ_{11}, δ_{22}, and Φ) grid search to see if we could find CSA tensors that fit the cytosine C5 and guanine C8 RCSAs to within experimental uncertainty. In both cases, the δ_{33} orientation (two parameters) was assumed normal to the base plane. CSA tensors were accepted if they reproduced (using Eq. (1) and the RDC-derived order tensors) the measured RCSAs to within a cut-off that includes the uncertainty in the measured RCSA (0.8 Hz) and RDC-derived order tensor ($\pm 5\%$ and ± 0.1 variations in GDO and η, respectively). These calculations were repeated millions of times each time following application of ca. 6° random Gaussian perturbations in the orientation of each base to account for structural noise. The average and standard deviations in the CSA parameters over the accepted solutions are listed in Table 1 (“RCSA”). For both cytosine C5 and guanine C8, CSA parameters could be obtained that reproduce all measured RCSAs to within experimental precision

(rmsd < 0.8 Hz, $Q < 20\%$, Fig. 4D and Table 1). Differences are however observed between the RCSA-derived principal values and Φ angles and the corresponding mononucleotide values (Table 1). We avoid interpreting the differences in Φ since simulations using synthetic C5 and C8 RCSAs show this angle to be intrinsically difficult to define on the basis of the RCSAs measured in TAR4312 (Table 1, Calc-4 and Calc-5). This is in part due to placement of the δ_{11} direction close to within the axially symmetric S_{xx}–S_{yy} plane of the order tensor. Nevertheless, we note that the deviations in Φ from the corresponding mononucleotide values are larger for cytosine C5 (~50°) compared to guanine C8 (~24°).

In contrast to Φ, simulations employing synthetic data show that the cytosine C5 and guanine C8 CSA principal values can be defined to a useful level of precision (~±16 ppm) using the measured RCSAs (Table 1, Calc-4 and Calc-5, respectively). The mean cytosine C5 CSA magnitude obtained using the RCSA grid search ($CSA_a = 173 \pm 21$ ppm) is significantly higher than all of the values reported for mononucleotides (131–138 ppm). In contrast, the RCSA-derived CSA_a value for guanine C8 (148 ± 13 ppm) is only slightly higher than the mononucleotide values and within experimental uncertainty equal to that of SS (134 ppm).

A number of factors suggest that the observed differences between the mononucleotide C5 CSA_a values and that derived here using RCSAs reflect genuine differences in C5 electron density in the mononucleotide and polynucleotide base. First, we note that the RCSA-derived CSA parameters for cytosine C5 leads to a better fit between the measured and back-calculated uridine C5 RCSAs (Fig. 4D, squares). The rmsd decreases from 1.6 to 0.6 Hz and the Q-factor from 48 to 14%. It is also noteworthy that the larger RCSA-derived C5 CSA_a value is comparable to that reported for pyrimidine C6 by SS and DFT2 (179–184 ppm). Unlike C5, a good fit is observed between the four measured C6 RCSAs and the SS and DFT2 CSAs (Table 1). Our results therefore suggest that the pyrimidine C5 and C6 have similar CSA_a values. Second, it is noteworthy that previous DFT calculations have shown that the CSA principal values of cytosine C5 are particularly sensitive to intermolecular interactions [23]. Finally, the larger cytosine C5 CSA_a value obtained here may explain some of the anomalously high order parameters ($S^2 \sim 1$) recently obtained for a number of C5 sites in RNA Watson–Crick base pairs [21]. These large order parameters could have arisen from use of what would have been an underestimated SS input CSA_a value in analyzing the C5 relaxation data [21].

In contrast to most spin relaxation measurements, which depend quadratically on CSA_a, RCSAs scale linearly with the CSA principal values. While this makes RCSA-based definition of the CSA tensor more difficult, it also means that the structural interpretation of RCSAs can tolerate a greater deal of CSA uncertainty. Indeed, SS, DFT1 and DFT2 CSAs all yield an overall RCSA fit to the TAR4312 structure (rmsd < 1.4 Hz, Fig. 4C) that is approximately an order of magnitude smaller than the predicted RCSA range (−10 to 10 Hz). This suggests that all of the measured RCSAs, including adenine C2 and C8, can be translated into useful "loose" structural constraints even after accommodating some uncertainty in the CSAs. Such uncertainty would also take into account potential site-specific variations in the CSA. What makes nucleobase RCSAs particularly attractive structural parameters is that they provide constraints on the δ_{33} principal direction which is oriented normal to the base along a direction seldom sampled directly by RDC interaction vectors, as shown in the inset of Fig. 4C for TAR4312.

To illustrate the utility of RCSAs as structural constraints, we examined the range of cytosine and guanine base orientations that are allowed by RDC and RDC + RCSA measurements. For each case, a domain-

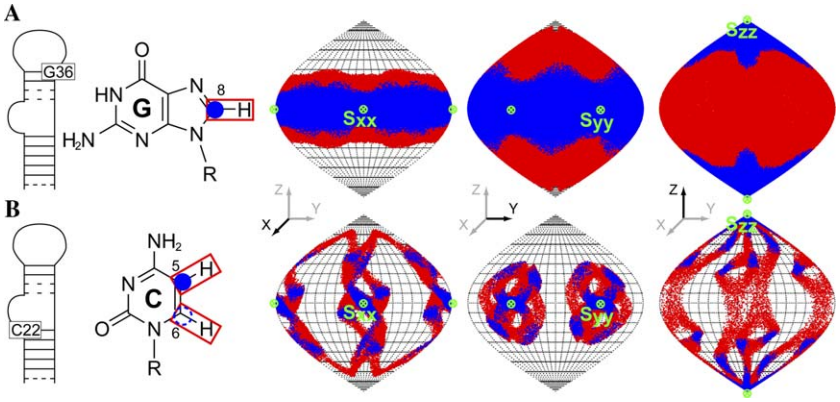

Fig. 5. Long-range constraints on the orientation of nucleobases from ^{13}C RCSAs. Sauson–Flamsteed projection maps showing the RDC (in red) and RDC + RCSA (in blue) allowed base orientations for (A) G36 (one RDC and one RCSA) and (B) C22 (two RDCs and one RCSA). The base orientations are depicted relative to the order tensor PAS (S_{xx}, S_{yy}, S_{zz}) derived for TAR4312 using RDCs (poles of map, depicted in green). Clustering of solutions around the poles of the map implies agreement with the RDC validated A-form structures. The reduction in the spread of RDC solutions (in red) upon inclusion of RCSAs (in blue) reflects how much better base orientations can be defined by RCSAs even in the presence of ~10–20% CSA uncertainty (see main text).

specific order tensor was derived using RDCs excluding values belonging to the residue examined. Next, all allowed base orientations were interrogated for their ability to back calculate RDCs or both RDC + RCSAs. Base orientations were accepted if the differences between the measured and predicted RDCs (or both RDCs and RCSAs) were smaller than a specified cut-off comprising errors in the measurement (1.4 and 0.8 Hz for RDCs and RCSAs, respectively), order tensor (±5% and ±0.1 variations in GDO and η, respectively), and CSA tensor (±10%, ±0.15, and ±20° variations in CSA_a, η, and Φ, respectively). The input CSA parameters were centered around the RCSA-derived values (RCSA, Table 1) but their uncertainty leads to CSA_a values that span those of DFT1, DFT2, and SS. Similar results were also obtained when centering the CSA parameters around the DFT1 or SS values (data not shown). As shown in Fig. 5A, a single C8–H8 RDC only partially restricts the allowed orientations of the G36 nucleobase. This is because in addition to the taco-shaped continuous distribution of orientations [50], rotations about the C8–H8 RDC bond vector itself are allowed leading to poor definition of the orientation normal to the base plane. Including an orthogonal constraint from a single C8 RCSA measurement greatly helps reduce the allowed orientations even after allowing for the aforementioned CSA uncertainty. As would be expected, the orientational solutions cluster closely around the poles of the map and hence orientation of the base in the RDC-validated A-form structure. For C22, the addition of a single C5 RCSA to two RDCs also substantially restricts the allowed continuous orientational solutions (Fig. 5B). Similar results were obtained for all other C2, C5, C6, and C8 RCSAs when using any of the mononucleotide CSAs and similar CSA uncertainty (data not shown).

3. Conclusion

The RCSAs measured in TAR4312 argue that the CSA magnitude (CSA_a) of cytosine C5 in A-form RNA under solution NMR conditions is larger than that previously reported for mononucleotides. In contrast, the RCSAs largely support the validity of the mononucleotide guanine C8 CSA_a value reported by solid-state NMR. Even after allowing for substantial uncertainty in the CSAs (ca. 10–20%), the RCSAs could be translated into useful long-range base-centered orientational constraints. This is in part because RCSAs provide constraints on directions orthogonal to the base plane that are seldom sampled directly by RDC vectors. Such constraints can in principle be obtained from additional measurements of other nucleobase one bond and two bond RDCs [51–53]. However, at the available magnetic field strengths, the field dependent RCSAs are between 4 and 15 times larger in magnitude and can be measured using sensitive NMR experiments that do not require resolution of small multiplet components. This will prove to be an advantage when studying larger RNAs.

Acknowledgments

We thank members of the Al-Hashimi laboratory for insightful comments, Dr. Jiri Czernek for providing us with the unpublished DFT2 C2 and C5 CSAs [25], and Dr. Kurochkin for NMR expertise. Funding from NIH (RO1 AI066975-01) and a Ralph E. Powe Junior Faculty enhancement award is acknowledged. The authors also acknowledge the Michigan Economic Development Cooperation and the Michigan Technology Tri-Corridor for the support of the purchase of a 600 MHz spectrometer.

References

[1] B. Reif, M. Hennig, C. Griesinger, Direct measurement of angles between bond vectors in high-resolution NMR, Science 276 (1997) 1230–1233.
[2] E. Chiarparin, P. Pelupessy, R. Ghose, G. Bodenhausen, Relative orientation of (CH alpha)-H-alpha-bond vectors of successive residues in proteins through cross-correlated relaxation in NMR, J. Am. Chem. Soc. 122 (2000) 1758–1761.
[3] H. Schwalbe, T. Carlomagno, M. Hennig, J. Junker, B. Reif, C. Richter, C. Griesinger, Cross-correlated relaxation for measurement of angles between tensorial interactions, Methods Enzymol. 338 (2001) 35–81.
[4] E. Duchardt, C. Richter, O. Ohlenschlager, M. Gorlach, J. Wohnert, H. Schwalbe, Determination of the glycosidic bond angle chi in RNA from cross-correlated relaxation of CH dipolar coupling and N chemical shift anisotropy, J. Am. Chem. Soc. 126 (2004) 1962–1970.
[5] D. Fushman, R. Xu, D. Cowburn, Direct determination of changes of interdomain orientation on ligation: Use of the orientational dependence of N-15 NMR relaxation in Abl SH(32), Biochemistry 38 (1999) 10225–10230.
[6] C.D. Kroenke, M. Rance, A.G. Palmer, Variability of the N-15 chemical shift anisotropy in Escherichia coli ribonuclease H in solution, J. Am. Chem. Soc. 121 (1999) 10119–10125.
[7] K. Pervushin, R. Riek, G. Wider, K. Wuthrich, Attenuated T-2 relaxation by mutual cancellation of dipole- dipole coupling and chemical shift anisotropy indicates an avenue to NMR structures of very large biological macromolecules in solution, Proc. Natl. Acad. Sci. USA 94 (1997) 12366–12371.
[8] X. Feng, M. Eden, A. Brinkmann, H. Luthman, L. Eriksson, A. Graslund, O.N. Antzutkin, M.H. Levitt, Direct determination of a peptide torsional angle psi by double-quantum solid-state NMR, J. Am. Chem. Soc. 119 (1997) 12006–12007.
[9] R.Q. Fu, T.A. Cross, Solid-state nuclear magnetic resonance investigation of protein and polypeptide structure, Annu. Rev. Biophys. Biomol. Struct. 28 (1999) 235–268.
[10] S.J. Opella, F.M. Marassi, Structure determination of membrane proteins by NMR spectroscopy, Chem. Rev. 104 (2004) 3587–3606.
[11] C.R. Sanders, B.J. Hare, K.P. Howard, J.H. Prestegard, Magnetically-oriented phospholipid micelles as a tool for the study of membrane-associated molecules, Prog. Nucl. Magn. Reson. Spectrosc. 26 (1994) 421–444.
[12] A. Ramamoorthy, S.J. Opella, Two-dimensional chemical shift/heteronuclear dipolar coupling spectra obtained with polarization inversion spin exchange at the magic angle and magic-angle sample spinning (PISEMAMAS), Solid State Nucl. Magn. Reson. 4 (1995) 387–392.
[13] G. Cornilescu, A. Bax, Measurement of proton, nitrogen, and carbonyl chemical shielding anisotropies in a protein dissolved in a dilute liquid crystalline phase, J. Am. Chem. Soc. 122 (2000) 10143–10154.
[14] Z.R. Wu, N. Tjandra, A. Bax, P-31 chemical shift anisotropy as an aid in determining nucleic acid structure in liquid crystals, J. Am. Chem. Soc. 123 (2001) 3617–3618.

[15] D.L. Bryce, A. Grishaev, A. Bax, Measurement of ribose carbon chemical shift tensors for A-form RNA by liquid crystal NMR spectroscopy, J. Am. Chem. Soc. 127 (2005) 7387–7396.
[16] J.R. Williamson, S.G. Boxer, Multinuclear NMR studies of DNA hairpins. 1. Structure and dynamics of d(CGCGTTGTTCGCG), Biochemistry 28 (1989) 2819–2831.
[17] C. Kojima, A. Ono, M. Kainosho, T.L. James, DNA duplex dynamics: NMR relaxation studies of a decamer with uniformly 13C-labeled purine nucleotides, J. Magn. Reson. 135 (1998) 310–333.
[18] K.B. Hall, C.G. Tang, C-13 relaxation and dynamics of the purine bases in the iron responsive element RNA hairpin, Biochemistry 37 (1998) 9323–9332.
[19] S. Ravindranathan, C.H. Kim, G. Bodenhausen, Cross correlations between 13C-1H dipolar interactions and 15N chemical shift anisotropy in nucleic acids, J. Biomol. NMR 27 (2003) 365–375.
[20] E. Duchardt, H. Schwalbe, Residue specific ribose and nucleobase dynamics in the cUUCGg RNA tetraloop motif by 13C relaxation, J. Biomol. NMR 32 (2005) 295–308.
[21] Z. Shajani, G. Varani, 13C NMR relaxation studies of RNA base and ribose nuclei reveal a complex pattern of motions in the RNA binding site for human U1A protein, J. Mol. Biol. 349 (2005) 699–715.
[22] M. Akke, R. Fiala, F. Jiang, D. Patel, A.G. Palmer, Base dynamics in a UUCG tetraloop RNA hairpin characterized by N-15 spin relaxation: correlations with structure and stability, RNA 3 (1997) 702–709.
[23] D. Stueber, D.M. Grant, 13C and (15)N chemical shift tensors in adenosine, guanosine dihydrate, 2′-deoxythymidine, and cytidine, J. Am. Chem. Soc. 124 (2002) 10539–10551.
[24] D. Sitkoff, D.A. Case, Theories of chemical shift anisotropies in proteins and nucleic acids, Prog. NMR Spectrosc. 32 (1998) 165–190.
[25] R. Fiala, J. Czernek, V. Sklenar, Transverse relaxation optimized triple-resonance NMR experiments for nucleic acids, J. Biomol. NMR 16 (2000) 291–302.
[26] J. Czernek, R. Fiala, V. Sklenar, Hydrogen bonding effects on the N-15 and H-1 shielding tensors in nucleic acid base pairs, J. Magn. Reson. 145 (2000) 142–146.
[27] A. Poon, J. Birn, A. Ramamoorthy, How does an amide-N-15 chemical shift tensor vary in peptides? J. Phys. Chem. B 108 (2004) 16577–16585.
[28] J. Boyd, C. Redfield, Characterization of N-15 chemical shift anisotropy from orientation-dependent changes to N-15 chemical shifts in dilute bicelle solutions, J. Am. Chem. Soc. 121 (1999) 7441–7442.
[29] R.S. Lipsitz, N. Tjandra, 15N chemical shift anisotropy in protein structure refinement and comparison with NH residual dipolar couplings, J. Magn. Reson. 164 (2003) 171–176.
[30] J. Kurita, H. Shimahara, N. Utsunomiya-Tate, S. Tate, Measurement of 15N chemical shift anisotropy in a protein dissolved in a dilute liquid crystalline medium with the application of magic angle sample spinning, J. Magn. Reson. 163 (2003) 163–173.
[31] R.S. Lipsitz, N. Tjandra, Carbonyl CSA restraints from solution NMR for protein structure refinement, J. Am. Chem. Soc. 123 (2001) 11065–11066.
[32] N. Tjandra, A. Bax, Direct measurement of distances and angles in biomolecules by NMR in a dilute liquid crystalline medium, Science 278 (1997) 1111–1114.
[33] J.R. Tolman, J.M. Flanagan, M.A. Kennedy, J.H. Prestegard, Nuclear magnetic dipole interactions in field-oriented proteins—information for structure determination in solution, Proc. Natl. Acad. Sci. USA 92 (1995) 9279–9283.
[34] P. Ram, J.H. Prestegard, Magnetic-field induced ordering of bile-salt phospholipid micelles - new media for Nmr structural investigations, Biochim. Biophys. Acta 940 (1988) 289–294.
[35] S. Gaemers, A. Bax, Morphology of three lyotropic liquid crystalline biological NMR media studied by translational diffusion anisotropy, J. Am. Chem. Soc. 123 (2001) 12343–12352.
[36] A. Meissner, J.O. Duus, O.W. Sorensen, Spin-state-selective excitation. Application for E.COSY-type measurement of J(HH) coupling constants, J. Magn. Reson. 128 (1997) 92–97.
[37] A. Meissner, O.W. Sorensen, The role of coherence transfer efficiency in design of TROSY-type multidimensional NMR experiments, J. Magn. Reson. 139 (1999) 439–442.
[38] M.R. Hansen, L. Mueller, A. Pardi, Tunable alignment of macromolecules by filamentous phage yields dipolar coupling interactions, Nat. Struct. Biol. 5 (1998) 1065–1074.
[39] G.M. Clore, M.R. Starich, A.M. Gronenborn, Measurement of residual dipolar couplings of macromolecules aligned in the nematic phase of a colloidal suspension of rod- shaped viruses, J. Am. Chem. Soc. 120 (1998) 10571–10572.
[40] A.J. Dingley, S. Grzesiek, Direct observation of hydrogen bonds in nucleic acid base pairs by internucleotide (2)J(NN) couplings, J. Am. Chem. Soc. 120 (1998) 8293–8297.
[41] J.A. Losonczi, M. Andrec, M.W.F. Fischer, J.H. Prestegard, Order matrix analysis of residual dipolar couplings using singular value decomposition, J. Magn. Reson. 138 (1999) 334–342.
[42] E. Ennifar, A. Nikulin, S. Tishchenko, A. Serganov, N. Nevskaya, M. Garber, B. Ehresmann, C. Ehresmann, S. Nikonov, P. Dumas, The crystal structure of UUCG tetraloop, J. Mol. Biol. 304 (2000) 35–42.
[43] H.M. Al-Hashimi, Y. Gosser, A. Gorin, W. Hu, A. Majumdar, D.J. Patel, Concerted motions in HIV-1 TAR RNA may allow access to bound state conformations: RNA dynamics from NMR residual dipolar couplings, J. Mol. Biol. 315 (2002) 95–102.
[44] H.M. Al-Hashimi, S.W. Pitt, A. Majumdar, W. Xu, D.J. Patel, Mg^{2+}-induced variations in the conformation and dynamics of HIV-1 TAR RNA probed using NMR residual dipolar couplings, J. Mol. Biol. 329 (2003) 867–873.
[45] S.W. Pitt, A. Majumdar, A. Serganov, D.J. Patel, H.M. Al-Hashimi, Argininamide binding arrests global motions in HIV-1 TAR RNA: comparison with Mg^{2+}-induced conformational stabilization, J. Mol. Biol. 338 (2004) 7–16.
[46] S.W. Pitt, Q. Zhang, D.J. Patel, H.M. Al-Hashimi, Evidence that electrostatic interactions dictate the ligand-induced arrest of RNA global flexibility, Angew Chem. Int. Ed. Engl. 44 (2005) 3412–3415.
[47] W.D. Cornell, P. Cieplak, C.I. Bayly, I.R. Gould, K.M. Merz, D.M. Ferguson, D.C. Spellmeyer, T. Fox, J.W. Caldwell, P.A. Kollman, A 2nd generation force-field for the simulation of proteins, nucleic-acids, and organic-molecules, J. Am. Chem. Soc. 117 (1995) 5179–5197.
[48] G.M. Clore, D.S. Garrett, R-factor, free R, and complete cross-validation for dipolar coupling refinement of NMR structures, J. Am. Chem. Soc. 121 (1999) 9008–9012.
[49] J.R. Tolman, H.M. Al-Hashimi, L.E. Kay, J.H. Prestegard, Structural and dynamic analysis of residual dipolar coupling data for proteins, J. Am. Chem. Soc. 123 (2001) 1416–1424.
[50] B.E. Ramirez, A. Bax, Modulation of the alignment tensor of macromolecules dissolved in a dilute liquid crystalline medium, J. Am. Chem. Soc. 120 (1998) 9106–9107.
[51] L. Zidek, H. Wu, J. Feigon, V. Sklenar, Measurement of small scalar and dipolar couplings in purine and pyrimidine bases, J. Biomol. NMR 21 (2001) 153–160.
[52] C.P. Jaroniec, J. Boisbouvier, I. Tworowska, E.P. Nikonowicz, A. Bax, Accurate measurement of 15N-13C residual dipolar couplings in nucleic acids, J. Biomol. NMR 31 (2005) 231–241.
[53] J. Yan, T. Corpora, P. Pradhan, J.H. Bushweller, MQ-hCN-based pulse sequences for the measurement of 13C1′-1H1′, 13C1′-15N, 1H1′-15N, 13C1′-13C2′, 1H1′-13C2′,13C6/8-1H6/8, 13C6/8-15N, 1H6/8-15N, 13C6-13C5, 1H6-13C5 dipolar couplings in 13C, 15N-labeled DNA (and RNA), J. Biomol. NMR 22 (2002) 9–20.
[54] R. Lavery, K. Zakrzewska, Base and base pair morphologies, helical parameters, and definitions, in: S. Neidle (Ed.), Oxford Handbook of Nucleic Acid Structure, Oxford University Press, New York, 1999, pp. 39–76.
[55] P. Vallurupalli, L.E. Kay, A suite of 2H NMR spin relaxation experiments for the measurement of RNA dynamics, J. Am. Chem. Soc. 127 (2005) 6893–6901.